An Experimental Study of Wi-Fi Joint Transmission with Multiple Openwifi Access Points

Baiheng Chen, Xianjun Jiao, Wei Liu, Thijs Havinga and Ingrid Moerman
IDLab, *Department of Information Technology*, Ghent University - imec, Ghent, Belgium
Email: {colvin.chen, xianjun.jiao, wei.liu, thijs.havinga, ingrid.moerman}@UGent.be

***Abstract*—Multi-Access Point Collaboration (MAPC) envisioned in future Wi-Fi standards has the potential to provide reliable connectivity for time-critical IoT applications. The joint transmission (JT) concept strengthens the signals at the station transmitted from distributed APs, increasing its resilience against interference and multi-path fading to improve reliability and latency performance. There is no commercially available Wi-Fi device capable of doing this since individual APs must be synchronized for time, RF carrier and packet data, and are required to share the medium access with each other. We present an experimental study of distributed dual-AP Wi-Fi network prototype with SDR platforms with *openwifi*. By synchronizing the clock source, packet transmission control and data, we demonstrate a successful constructive overlap of transmitted Wi-Fi signals at the receiver from distributed APs. Specifically, we observe a $6\,\mathrm{dB}$ received signal power gain and a $4.4\,\mathrm{dB}$ SNR improvement from the decoded packets with two APs compared to a standalone transmission in the experiment.**

***Index Terms*—Wi-Fi, IEEE 802.11, IoT, Joint Transmission, FPGA, Multi-AP Coordination, Wireless Communication**

I. Introduction

Recently, Wi-Fi (IEEE 802.11) has received increased attention in machine-to-machine (M2M) connections thanks to the rapid growth of Internet of Things (IoT) applications. The advantage of low deployment cost and extensive IoT support helped Wi-Fi claim 31% of global IoT connections in 2023; the other two main technologies Bluetooth and cellular shared 25% and 21%, respectively [1]. Time-critical IoT applications are envisioned as a crucial driver of future development and a key market enabler; these applications require simultaneously low latency ($<10\,\mathrm{ms}$), high throughput (up to $>25\,\mathrm{Mbps}$ for real-time video streaming-based applications) and high reliability ($>$99.9%) from their connectivity, and are often tied to short-range and indoor scenarios [2], [3] where Wi-Fi usage dominates over other wireless communication standards with a 60% share of all indoor wireless traffic [4].

Wi-Fi has been continuously evolving towards preparing for time-critical applications. Previously, extensively contended Wi-Fi packets with the current Carrier Sense Multiple Access with Collision Avoidance (CSMA/CA) medium access control (MAC) protocol can quickly saturate the channel in dense deployments, resulting in the failure of timely packet delivery [5]. Higher throughput packets modulate symbols in a denser constellation but will also be more prone to multi-path fading and interference, which is common in indoor IoT traffic. A packet failed to be delivered or not decoded in time results in re-transmissions, during which other stations (STAs) cannot transmit their queued packets; the added the overall latency is unpredictable and deadly for time-critical scenarios. Such problems can severely hinder the Wi-Fi-based IoT performance. To address these problems, new Wi-Fi standards use techniques such as orthogonal frequency-division multiple access (OFDMA) and multi-link operation (MLO) [6] to substantially improve throughput [7] and latency performance [8].

IEEE 802.11bn amendment, the next generation Wi-Fi 8, is foreseen to introduce multi-access point cooperation (MAPC) where individual access points operate in a coherent manner for increased reliability [9]. Joint transmission (JT) is one of the MAPC techniques and allows the spatially distributed APs to simultaneously transmit to the stations. Properly steered APs can constructively overlap packets at targeted STAs for improved received power and spatial diversity, and boosted SNR [10]. Compared to traditional co-located single AP beamforming and MIMO technology, distributed APs extend the service range, minimize blind spots, and convert inter-AP interference into gain in complex indoor venues such as shopping malls and automated factories, in which the IoT applications are bountiful and their timely operation is desired. With JT, each receiver (RX) sees the distributed transmitters (TX) as a single virtual, powerful, and directional antenna with optimal transmission conditions. This helps boost received signal power and hardens the channel to reduce packet error rate for higher reliability in a complex environment [10], thus also reducing re-transmissions and improving overall latency performance. To achieve JT with Wi-Fi, distributed APs must overcome the following technical challenges [11], [12], [13]:

- The sampling clock and radio frequency (RF) clock in each AP must be synchronized with each other.
- Baseband operations in distributed APs must be synchronized and aligned in time.
- APs need to transmit in the same channel simultaneously.
- Client-specific packet data to be transmitted shall be known at every AP before transmission.

To the best of our knowledge, there are currently neither commercial off-the-shelf (COTS) JT-ready Wi-Fi chips, nor fully prototyped implementations. Wi-Fi operations such as preparing acknowledgments have to be done in real-time in hardware due to Wi-Fi's tight time constraints; modifying COTS chips for achieving JT is costly and takes long time.

The open source full stack Wi-Fi design *openwifi* [14] based on software-defined radio (SDR) and field programmable gate array (FPGA) platform provides full access to the baseband hardware design and is widely used for academic and research activities. For the capability of baseband modification through FPGA and software support, we believe openwifi has the best potential for early prototyping and validating JT with Wi-Fi.

The IEEE 802.11 working group has approved that the MAPC coordinated beamforming transmission will be limited to only two APs in the upcoming 802.11bn amendment [15]. The motion is proposed to limit the transmission overhead and reduce implementation complexity. We believe an early validation and prototyping of dual-AP JT is necessary to evaluate the potential strength of the technology. Advancing JT beyond two APs is very promising; yet it is not envisioned in the upcoming Wi-Fi standard due to the exponentially growing complexity and implementation difficulty. We therefore consider JT with more than two APs as our main future goal.

In this paper, we present an experimental work using openwifi-based SDR platform to demonstrate and prove the viability of dual-AP Wi-Fi JT with a simple setup. We emphasize the necessity of a synchronized clock source in multi-AP scenario to achieve RF and sample-level synchronization between APs. We conduct simulations and measurements between the APs and the client, and evaluate the link quality of the received signal in terms of its power and signal-to-noise-ratio (SNR) reflected through Error Vector Magnitude (EVM) measurements.

The rest of the paper is organized as follows: Section II shows the related works in JT. Section III presents the mathematical theories involved, and our methods used to achieve JT with openwifi, with details of the simulation conducted. Section IV presents the simulation process, the hardware experiment setup and the results obtained. Section V concludes the significance of this work, while setting forth a future research plan.

II. Related Works

Authors of [12] present a joint transmission with a phase-error-resilient precoding scheme in Wi-Fi 7 and beyond. Even through presented with promising simulation results, the mentioned studies are generally constrained in theoretical field and lack practical implementation and validation. Particularly, most of the studies do not address the impact of nonideal AP synchronization in the simulators. This work presents a multi-AP joint transmission design from theory to implementation and pays attention to clock synchronization between APs. Reference [13] presents a comprehensive survey of MAPC with respect to Wi-Fi 7 outlook including JT. Although MAPC may not be standardized in Wi-Fi 7, the survey outlines the foreseen applications and challenges to be introduced in Wi-Fi 8. In [16] the authors present a distributed multiple-input-multiple-output (MIMO) architecture for Wi-Fi APs dedicated for office environment using Wi-Fi 6. Reference [17] and [18] discuss the benefit of spatial reuse enabled by coordinated Wi-Fi APs.

Through simulation and cable-based hardware tests, we present a validation of JT using 802.11n-compatible PHY and MAC with low cost development boards. MegaMIMO 2.0 [19] has the closest scope to our work. The authors demonstrate distributed transmission by showing a 3.6 times higher throughput with 4×4 MegaMIMO nodes compared to a single 802.11 link; Triggering transmission on distributed APs is done through over-the-air packets. In our work, we verify the design using physical layer (PHY) metrics of measured power gain and SNR improvement from the overlapped signals instead of throughput. Additionally, we trigger packet transmission on distributed APs through cabled interface, emulating a dedicated backbone design, which is a more friendly solution for time-critical IoT applications with less over-the-air overhead.

III. Theory and Methodology

A. Channel model and metric

We consider the downlink traffic in a distributed multi-AP network and assume each AP and the client has only one TX antenna and one RX antenna. The downlink channel is equivalent to a multiple-input-single-output (MISO) channel model expressed in (1). The received time-domain symbol y with noise n is hence the vector sum of transmitted symbol x_M from M paths each with channel response h_M.

$$y = \sum_{m=1}^{M} (h_m * x_m + n_{\text{TX},m}) + n_{\text{RX}} = y_{\text{RX}} + n \quad (1)$$

where $n = \sum_{m=1}^{M} n_{\text{TX},m} + n_{\text{RX}}$ and n is added white Gaussian noise (AWGN). n_{TX} and n_{RX} are noise contributed by the TX chain and RX chain respectively and both are AWGN. Specifically, even with a perfect digital baseband signal, TX noises can still arise from the analog and RF components in individual devices. These can include phase noise in the oscillator, thermal noise, quantization noise and power supply noise. As the number of TX grows, the TX noise component can become significant. Hence we describe the channel SNR as in (2) for a distributed MISO scenario, where $P(\cdot)$ denotes the power of a signal for simplicity.

$$\text{SNR}_{\text{MISO,dB}} = 10 \cdot \log_{10}\left(\frac{P_{y_{\text{RX}}}}{P_n}\right) \quad (2)$$

In this study we do not consider optimum power allocation and limit the scope to where APs always have the same TX power. On constructive overlap, $P_{y_{\text{RX}}} \propto M^2$ if x_m and h_m are identical in all M paths. In a coherent 2×1 MISO system with constructive overlap, $P_{y_{Rx}}$ increases by four times or $6\,\text{dB}$. Depending on the noise performance of TX and RX device, two extreme cases exist:

- RX noise dominates over TX noise, $n_{\text{RX}} \gg n_{\text{TX}}$.
- TX noise dominates over RX noise, $n_{\text{TX}} \gg n_{\text{RX}}$.

Introducing one additional AP results in P_n increasing by $0\,\text{dB}$ (unchanged) and $3\,\text{dB}$ (doubled) for the two extreme cases if both noise are AWGN, hence $\text{SNR}_{\text{MISO,dB}}$ increases by $6\,\text{dB}$ and $3\,\text{dB}$, respectively. However, n_{TX} and n_{RX} relationship can

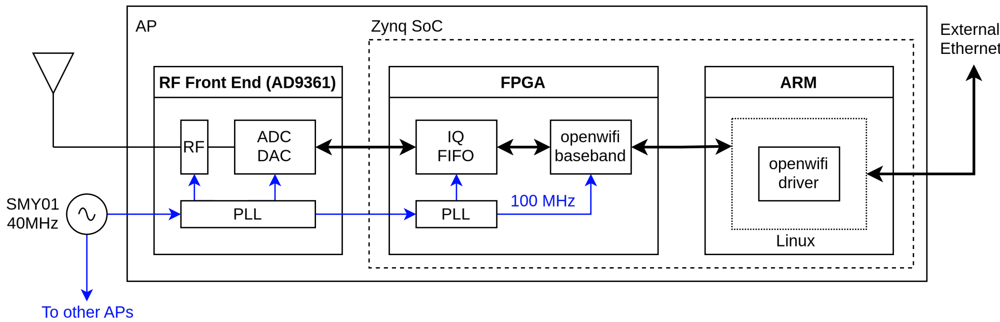

Fig. 1. Openwifi-based AP architecture. Blue lines are clock connections.

differ for different devices, so the 2-TX constructive overlap SNR improvement can range anywhere between 3 dB to 6 dB in a real world environment.

B. Platform preparation

We select *openwifi*-based SDR as our experiment platform for baseband customization towards JT. For this work we prepare two SDR boards as the AP, each consisting of a Xilinx Zynq Z-7035 System-on-Chip (SoC) for openwifi baseband and an Analog Devices AD9361 as the RF front end, as shown in Fig. 1. The SoC contains an ARM processing system that runs the openwifi driver in Linux kernel space, and a separate programmable logic unit serving as the FPGA.

We use a R&S®CMW270 Wireless Connectivity Tester as the client to receive and analyze the Wi-Fi signal from the APs. To benchmark JT performance, we evaluate the power and EVM result reported by CMW270. EVM measures the drift of a modulated symbol from its ideal constellation; the lower the EVM value, the better the modulation accuracy. In an AWGN channel using data-aided technology, change in EVM in dB is roughly inversely proportional to the change in SNR in dB [20]: a 3 dB SNR increase expects a 3 dB EVM decrease.

For the test data, we use the bit-true MATLAB model of openwifi transmitter to generate a Data packet of 802.11n (High-Throughput, HT) format with 256 bytes of payload data using modulation and coding scheme (MCS) 1, long guard interval and bandwidth of 20 MHz. Data bits are orthogonal frequency-division multiplexing (OFDM) modulated with 52 data subcarriers and 4 pilot subcarriers per OFDM symbol. Together with one DC subcarrier and 7 guard subcarriers, an OFDM symbol contains 64 subcarriers over the 20 MHz channel. This generated test packet is identical to a packet produced by real-time FPGA on-board openwifi baseband given the same MAC protocol data unit, and has been verified by COTS CMW270. Due to special precoding requirement for the experiment, we generate the packet offline instead of on-board. This will be further discussed in Section III-F.

The experiment is conducted via coax cables at 2500 MHz carrier frequency to avoid co-channel interference with ordinary 2.4 GHz traffic. Access control to the medium is performed as described in Section III-E. We configure the two APs as master-slave topology; Board-to-Board (BtB) connection is via a general purpose input and output (GPIO) port of the SDR board.

C. Clock synchronization

Individual crystal oscillators on electronic devices can randomly differ in frequency and phase; to eliminate the center frequency offset (CFO) and sampling frequency offset (SFO) between the two TXs, we use a common clock source for the two APs. In Fig. 1 the clock dependency on an openwifi AP is shown in blue-color. The ARM processor runs on a separate and independent clock and is omitted here. AD9361 is driven by a 40 MHz clock from a R&S®SMY01 signal generator; AD9361 internal phase-locked-loop (PLL) generates the RF carrier local oscillator (LO), the sampling clocks for TX and RX, and a separate clock signal to drive the FPGA. The FPGA PLL additionally generates a 100 MHz clock for openwifi baseband processing and the FIFO access to baseband samples. The FIFO outputs 20 MHz baseband samples to AD9361. Clock phase correction is performed using AD9361 native functionality [21] as a power-up routine. The synchronization trigger is generated in master AP in the form of a clocked pulse to indicate the correct clock transition timing. Slave AP receives the synchronization trigger through BtB connection.

D. Clock quality assessment

Main clock quality can severely impact the rest of the processing chain and result in SNR degradation in an OFDM-based system with phase noise (thus jitter) [22]. The larger the jitter, the worse quality the clock has, therefore the more noise associated with the signal generated. We measure the phase noise of the clock signal from the original SDR on-board crystal and SMY01 at 40 MHz using Anritsu MS2690A Signal Analyzer. Phase noise measurement presented in Table I is conducted at frequency offset from 10 Hz to 10 MHz at logarithmically spaced frequency points. An approximated phase noise plot can be constructed from the measurement, and is presented in Fig. 2 for the two sources respectively.

Conversion of measured phase noise to RMS clock jitter is done using (3) [23]. The approximated phase noise plot $L_\phi(f)$ can be piece-wise integrated (in linear scale, $1/\text{Hz}$) over the measured bandwidth to yield S, the area under curve in Fig. 2,

TABLE I

MEASURED PHASE NOISE OF THE ON-BOARD CRYSTAL AND SMY01 AT 40 MHz USING MS2690A ANALYZER.

Frequency Offset (Hz)	Phase Noise (dBc/Hz)	
	on-board Crystal	*SMY01*
10	-79.88	-73.15
100	-99.02	-67.06
1k	-104.33	-81.22
10k	-107.61	-107.83
100k	-112.85	-121.16
1M	-114.8	-138.05
10M	-128.44	-139.01

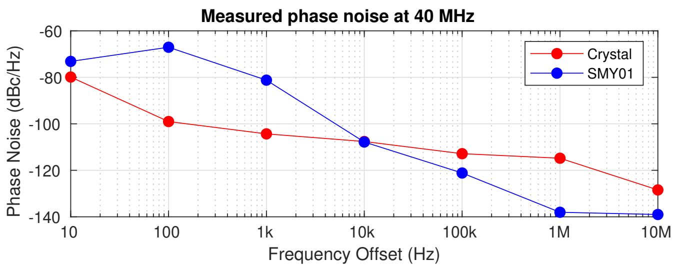

Fig. 2. Approximated phase noise plot at 40 MHz oscillator frequency using measured data from MS2690A for clock source on-board crystal and SMY01.

which is the sum of power ratios between the noise and the carrier over the finite frequencies measured. For this work, $f_{\text{start}} = 10\,\text{Hz}$, $f_{\text{end}} = 10\,\text{MHz}$ and $f_0 = 40\,\text{MHz}$.

$$\text{RMS Clock Jitter (sec)} = \frac{\sqrt{2S}}{2\pi f_0}, \text{ where } S = \int_{f_{\text{start}}}^{f_{\text{end}}} L_\phi(f)df \tag{3}$$

We evaluate the jitter to be 25.88 ps and 66.17 ps for the on-board crystal and SMY01 respectively; SMY01 jitter is approximately $2.5\times$ of on-board crystal jitter, hinting a worse clock performance if the SMY01 is used as the common clock. We use CMW270 to measure 100 packets transmitted standalone with each clock source to visualize and validate the impact of the increased clock jitter. Table II lists the relevant measurement results.

Given the device and the channel are unchanged, a 10 dB EVM degradation is observed when switching from on-board crystal to SMY01: the received symbols are more deviated and scattered from the constellation points. The crystal case has an average center frequency offset of $-59\,852.15$ Hz with standard deviation 68.2, whereas the SMY01 case has a lower average offset of 962.66 Hz but a higher standard deviation of 349.59. The symbol clock error is also more deviated. Given that frequency offset error carried over from the transmitter is easier to be corrected than jitter in the receiver, SMY01 can still be used as the common clock source, however, with an expectation of reduced EVM performance.

E. Coordinated medium access

Distributed APs need to occupy the medium and begin the packet transmission simultaneously to achieve JT, but uncoordinated CSMA/CA forbids this. Hence we modify openwifi low-MAC with the following principles to achieve distributed and coordinated CSMA/CA, and still be compliant with existing 802.11 MAC (not limited to 2 APs):

- There will be one master AP in the set of selected APs; other APs in the channel are slave APs.
- All APs are collectively treated as a single AP for CSMA in that channel for the client.
- The Master AP determines the transmit opportunity (TXOP). Slave APs do not decide on their TXOP.
- When the master AP (sharing AP) acquires a TXOP through CSMA, it notifies the slave APs (shared APs) to start the transmission simultaneously.

We use BtB link to deliver the transmit trigger generated in the master AP to the slave, emulating a low-latency backbone-based communication between APs. This ties the start of transmission on two APs together to the same real-time metric. When given the identical packet content, the two APs can transmit the same digital sample for every clock cycle.

TABLE II

CLOCK-RELATED MEASUREMENTS FROM TRANSMITTED WI-FI PACKETS USING CMW270 FOR FPGA WITH DIFFERENT CLOCK SOURCE.

Metric	on-board Crystal		SMY01	
	Mean	*StdDev*	*Mean*	*StdDev*
EVM All Subcarriers (dB)	-36.44	0.32	-26.08	0.47
Center Frequency Error (Hz)	-59852.15	68.2	962.66	349.59
Symbol Clock Error (ppm)	-23.095	0.415	-0.071	1.896

F. Mimicking sounding procedure and precoding

Openwifi AP currently does not have the capability to sound the transmission channel. The main objective of this work is to first verify JT functionality with two openwifi APs, therefore we consider sounding as the next step so we proceed with simple channel and supply the baseband with pre-calculated precoding vectors that emulates the sounded feedback.

Conjugate precoding is used in the APs to steer the packets to constructively overlap at the RX. Consider frequency domain transmitted data symbol X, channel response H and received data symbol Y: a single link AWGN channel is expressed as $Y = HX + N$. The precoding vector V can be used to steer X so that the TX transmits $V \cdot X$ instead of X. When V is ideal where $V = H^{-1}$, $Y = X + N$ and the RX effectively sees an AWGN channel. In a two-channel scenario, conjugate precoding can be used to steer the symbols transmitted over one channel (H_2) as if they are transmitted from the other path (H_1), by using $V_{1,2} = H_2^{-1} \cdot H_1$ as demonstrated in (4).

$$\begin{aligned} Y_{2,\text{new}} &= H_2(H_2^{-1} \cdot H_1 X) + N \\ &= H_1 X + N = Y_1 \end{aligned} \tag{4}$$

A complex multiplier is used as the generic baseband precoder. It treats the OFDM symbol with the precoding vector V, per subcarrier, to yield the precoded symbols before converting to time-domain samples through IFFT. In this experiment we want to verify the precise signal overlapping, which requires symbols from different channels to carry the same phase to observe the $6\,\mathrm{dB}$ power gain. Therefore we apply conjugate precoding to every field and OFDM symbol of the digital signal, in contrast to a standardized Wi-Fi MIMO transmission where only certain fields are precoded.

G. Transmission channel

For this work we use coax cables and an RF power combiner to form the channel between the APs and CMW270 tester, mimicking a simple and controlled AWGN channel. It is expressed in frequency domain with (5). $H_{\text{coax,ideal}}[k]$ and $A[k]$ are the channel response and complex channel gain at k^{th} subcarrier. $K = 64$ in HT packets; ideally, $A[k] = 1 \forall k$.

$$H_{\text{coax,ideal}}[k] = A[k] \;\forall\; k = 0, 1, \ldots, K-1 \tag{5}$$

Carrier phase offset (CPO) and sample timing error (STE) between the TX and the RX are inevitable in real world transmissions, since TX and RX are often independent devices and do not share a common clock. For an imperfectly sampled time-domain signal, CPO arises due to the phase difference between TX and RX RF clock; STE arises from phase offset in sampling clocks and results in nonideal sampling instances. We additionally model CPO and STE as part of the full transmission channel. $\omega \in [-\pi, \pi]$ describes the possible CPO between the TX AP and the RX. τ is the sampling delay factor accounting for STE and is in the unit of number of samples, which can be different for every power cycle. An optimally sampled signal at both TX and RX side has $\tau = 0$; a signal delayed by 1 sample has $\tau = 1$. The RX is capable of phase tracking to compensate for minor clock error, hence ω and τ acquired through channel estimation remain relatively constant for the duration of the transmission. The coax cable-formed channel with CPO and STE can thus be expressed in (6).

$$H_{\text{coax}}[k] = A[k] e^{-j(\omega + \frac{2\pi}{K} k\tau)} \tag{6}$$

Compared to (5), (6) introduces a unitary-magnitude term which carries the phase $-j(\omega + \frac{2\pi}{K} k\tau)$. This term results in a phase shift in every subcarrier. ω inflicts a constant global phase offset to all subcarriers, often called as common phase error (CPE); we intuitively address CPE as *offset*, deriving from its impact on the shape of the phase across all subcarriers. τ causes additional rotation per subcarrier that is proportional to k; the increment of phase shift per adjacent subcarrier is addressed as phase error gradient (PEG) $\delta = 2\pi\tau/K$. Similar to *offset*, a more intuitive name for PEG is *stepsize*, since it results in a stepped phase change per adjacent subcarrier and remains constant across all subcarriers. When $\tau = 1$ i.e. STE is exactly one sample in time domain, $|\delta_{\text{max}}| = 2\pi/64 = 0.098175\ \text{rad} = 5.625\ \text{deg}$. For a short-distance transmission office-environment setup, we assume worst case $\Delta\tau \in [-1, 1]$ where $\Delta\tau = \tau_1 - \tau_2$ between master and slave path and are fixed in a power cycle, so $\delta \in [-5.625, 5.625]$ deg. Fig. 3 is an example plot to intuitively show how nonzero ω and δ can impact the channel estimation from the Wi-Fi preamble. Note

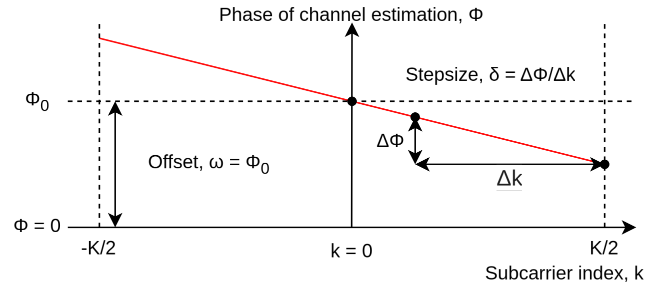

Fig. 3. An example phase plot versus subcarriers of channel estimation based on Wi-Fi preamble, in presence of CPE (*offset*, ω) and PEG (*stepsize*, δ).

that Fig. 3 is FFT-shifted; the center subcarrier with index 0 represents the DC component, and the indices of active subcarriers fall into $[-K/2, K/2]$.

With known ω and τ (hence δ) from the channel estimation, precoding vector V_{coax} for the coax cable-formed channel can be derived to compensate for CPO and STE over the transmission as (7).

$$V_{\text{coax}}[k] = \frac{1}{A[k]} e^{-j(-\omega - \frac{2\pi}{K} k\tau)} = \frac{1}{A[k]} e^{-j(-\omega - \delta k)} \tag{7}$$

so that $H_{\text{coax}}[k] V_{\text{coax}}[k] = 1\ \forall k$. In a dual-AP case, applying (4) with (7) between two coax cable-formed channels steers symbols transmitted through channel H_2 as if they are transmitted through H_1 in the RX perspective, as shown in (8).

$$V_{\text{coax},1,2}[k] = \frac{A_1[k]}{A_2[k]} e^{-j((\omega_1 - \omega_2) + (\delta_1 - \delta_2)k)} \tag{8}$$

IV. Simulation and On-Board Experiment

We simulate a 2×1 MISO model in MATLAB that follows (1) to visualize the constructively overlapping signal with our channel model. Two APs transmit to the RX via AWGN channels, $A_1[k] = A_2[k] = 1 \forall k$. Master path is assumed ideal hence $\tau_{\text{master}} = 0$ and $\omega_{\text{master}} = 0$ slave path has randomized τ and ω per power cycle to represent STE and CPO variation. For simplicity, precoding takes place at the slave AP only.

Table III shows the simulated power, EVM and actual SNR results of standalone transmission and dual-AP JT assuming perfect precoding at $30\,\mathrm{dB}$ single link SNR, for both TX-noise- and RX-noise dominating cases. A $6\,\mathrm{dB}$ power gain in each combined case can be observed, together with $3\,\mathrm{dB}$ EVM improvement with $3\,\mathrm{dB}$ SNR gain in TX-noise dominating simulation, and $6\,\mathrm{dB}$ EVM improvement with $6\,\mathrm{dB}$ SNR gain in RX-noise dominating case.

To imitate the absent sounding procedure, sweep simulation is performed with *offset* $\omega \in [-\pi, \pi]$ rad in steps of 0.05π rad to compensate $\omega_{\text{master}} - \omega_{\text{slave}}$ and *stepsize* $\delta \in [-5.65, 5.65]$ deg in steps of 0.05 deg to correct for $\frac{2\pi}{K}(\tau_{\text{master}} - \tau_{\text{slave}})$, the "unknown" STE and CPO. Precoding vector V at the slave AP is calculated for every ω-δ pair. The sweep simulation is conducted with $30\,\mathrm{dB}$ single link SNR for a TX-noise dominating scenario with a $3\,\mathrm{dB}$ expected

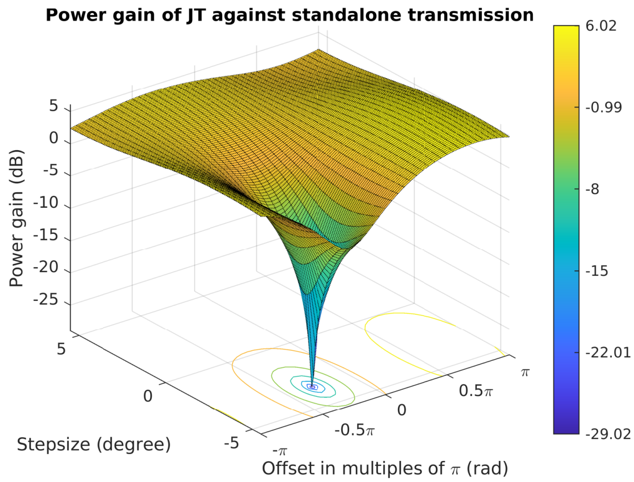

Fig. 4. Simulated power gain of JT compared to standalone transmission. A positive number indicates a higher (better) power received compared to standalone transmission.

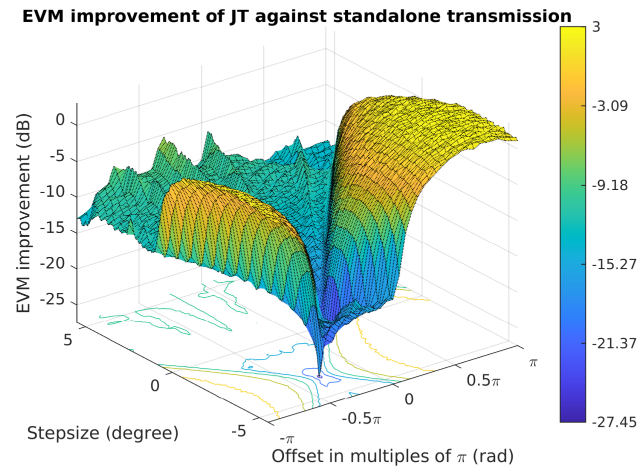

Fig. 5. Simulated EVM improvement of JT compared to standalone transmission. A positive number indicates a lower (better) EVM achieved compared to standalone transmission.

TABLE III
SIMULATION OF POWER, EVM AND ACTUAL SNR OF JT AND STANDALONE TRANSMISSIONS.

Metric		Standalone	Joint	Improvement
TX-noise dominating	Power (dBm)	29.96	35.98	6.02
	EVM (dB)	-28.03	-31.02	2.99
	Measured SNR (dB)	30.98	33.99	3.01
RX-noise dominating	Power (dBm)	29.96	35.98	6.02
	EVM (dB)	-28.03	-34.01	5.98
	Measured SNR (dB)	30.98	37.01	6.02

constructive overlap EVM improvement. We plot the power gain and the corresponding EVM improvement of JT packets composed of unprecoded master signal and precoded slave signal, against standalone packets from master AP in Fig. 4 and Fig. 5 respectively. The x- and y-axis values indicate the *offset* ω and *stepsize* δ associated with V at the slave AP.

In Fig. 4, a $6.02\,\text{dB}$ power gain is achieved at $\omega = 0.7\pi\,\text{rad}$ and $\delta = -3.5\,\text{deg}$; this combination also yields the peak of the EVM improvement plateau in Fig. 5 where the value is $3\,\text{dB}$. Given this is a TX-noise dominating AWGN simulation, the numbers thereby indicates that master and slave signals have constructively overlapped at the RX. A trough of nulled power is observed at at $\omega = -0.3\pi\,\text{rad}$ and $\delta = -3.5\,\text{deg}$ in Fig. 4, and corresponds to the most negative EVM improvement value in Fig. 5. Here the slave signal is out-of-phase with the master signal and completely cancels out with destructive overlap.

The experiment hardware setup is presented in Fig. 6. We use coax cables and an RF combiner to form two independent paths in the MISO AWGN channel. CMW270 is used to measure the power and EVM of the received signal and to evaluate the quality of dual-AP JT.

The same sweep test method in simulation is followed and precoding is limited to openwifi board 2 (slave AP) only. We locate the ω-δ combination that yields the most consistent

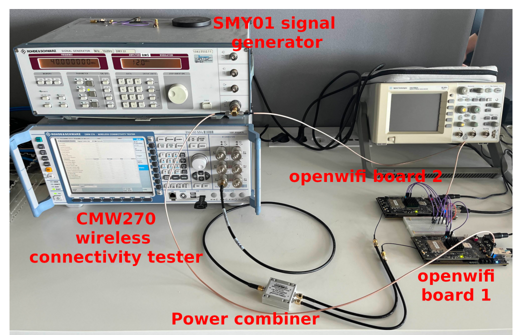

Fig. 6. Dual-AP JT experiment setup.

$6\,\text{dB}$ power gain reported by CMW270. A total of 1000 standalone packets and JT packets with the optimal precoding applied are then transmitted for verification. All 2000 packets have been detected and successfully decoded by CMW270. Table IV presents the average power and EVM statistics. A $6\,\text{dB}$ gain in both packet power and peak power is observed in Table IV. Note the EVM measurement of standalone packets is slightly higher than first measurement in Table II due to more packets measured. The power expectation for a constructive overlap of signals from two distributed APs is achieved. The statistics indicate the signals have been constructively overlapped as expected. SNR improvement implied from the measured average EVM improvement is $4.4\,\text{dB}$ which lies between $3\,\text{dB}$ for a TX-noise dominating case or $6\,\text{dB}$ for an RX-noise dominating case. We also observe the increase of $1.39\,\text{dB}$ in noise floor (more noisy) during JT compared to standalone transmission which may be the main cause of the $4.4\,\text{dB}$ SNR improvement. This can be due to the imperfect clock source SMY01 with high jitter. Additionally, we believe the setup has a nonideal noise performance where both TX

TABLE IV
MEASURED POWER AND EVM USING CMW270 FOR STANDALONE AND DUAL-AP JOINT TRANSMISSION FOR 1000 PACKETS EACH.

Metric	Standalone	Joint	Improvement
Packet Power (dBm)	-18.00	-11.99	6.01
Peak Power (dBm)	-8.45	-2.43	6.02
EVM All Subcarriers (dB)	-25.03	-29.43	4.40
Measured Noise Floor (dBm)	-57.82	-56.43	-1.39

and RX contribute a remarkable part of the overall noise. Specifically, we use a cabled channel with very low path loss so TX noise leakage can propagate to RX with little attenuation. In contrast, a normal over-the-air transmission would have much higher path loss which makes TX noise less significant in the received signal. In that case, a $6\,\mathrm{dB}$ SNR improvement is expected.

V. CONCLUSION

We show that two independent APs can be coordinated and synchronized to achieve sample-level phase coherency and RF synchronization for transmitting the same packet content simultaneously from distributed locations. By observing a $6\,\mathrm{dB}$ power gain and a $4.4\,\mathrm{dB}$ EVM improvement hence $4.4\,\mathrm{dB}$ SNR gain from the jointly transmitted packet over the coax-cable formed channel, we show a constructive overlap of signals at the client. Through this work we prove that JT over Wi-Fi is prototyped using simple low-cost SDR platforms. With this, we show that JT can be an effective and easily-deployable solution in future Wi-Fi standards in boosting the strength of transmission.

For future work, distributed MIMO channel sounding and AP scheduling are important next steps. Additionally, we aim to examine an effective backbone-based communication and time-synchronization protocol between APs for the shared data and control to replace current BtB solution. Using additional calibration process before joint transmission for reducing clock errors between slaves and master will be considered in the PHY. The JT experiment scope will be expanded to more than two APs to prepare for more complex network, and include over-the-air transmission and multi-path fading where it best reflects the real environment of time-critical IoT applications.

ACKNOWLEDGMENT

This work is partially funded by the Flemish FWO SBO S006224N SMART-STRIP, Methusalem SHAPE: Next Generation Wireless Networks under grant 20-MET-004, and HORIZON-ERC-POC DCAP (Distributed Coordinated Access Point) with project number 101158037.

REFERENCES

[1] S. Sinha, "State of iot 2024: Number of connected iot devices growing 13% to 18.8 billion globally," Sep 2024. [Online]. Available: https://iot-analytics.com/number-connected-iot-devices/

[2] "Ericsson mobility report," Ericsson AB, June 2024. [Online]. Available: https://www.ericsson.com/en/reports-and-papers/mobility-report/reports/june-2024

[3] F. Alriksson, L. Boström, J. Sachs, Y.-P. E. Wang, and A. Zaidi, "Critical iot for time-critical communications," Ericsson. [Online]. Available: https://www.ericsson.com/en/reports-and-papers/ericsson-technology-review/articles/critical-iot-connectivity

[4] "Cisco annual internet report," Cisco Systems, Inc., Mar 2020. [Online]. Available: https://www.cisco.com/c/en/us/solutions/executive-perspectives/annual-internet-report/index.html

[5] T. Adame, M. Carrascosa-Zamacois, and B. Bellalta, "Time-sensitive networking in ieee 802.11be: On the way to low-latency wifi 7," *Sensors*, vol. 21, no. 15, 2021.

[6] G. Naik, D. Ogbe, and J.-M. J. Park, "Can wi-fi 7 support real-time applications? on the impact of multi link aggregation on latency," in *ICC 2021 - IEEE International Conference on Communications*, 2021, pp. 1–6.

[7] R. d. Vegt, "Reduced latency benefits of wi-fi 6 ofdma," Wi-Fi Alliance. [Online]. Available: https://www.wi-fi.org/beacon/rolf-de-vegt/reduced-latency-benefits-of-wi-fi-6-ofdma

[8] D. Lopez-Perez, A. Garcia-Rodriguez, L. Galati-Giordano, M. Kasslin, and K. Doppler, "Ieee 802.11be extremely high throughput: The next generation of wi-fi technology beyond 802.11ax," *IEEE Communications Magazine*, vol. 57, no. 9, pp. 113–119, 2019.

[9] P. Imputato, S. Avallone, and D. Magrin, "Multi-ap coordination in wi-fi 7 exploiting time resources sharing," in *2022 IEEE International Mediterranean Conference on Communications and Networking (MeditCom)*, 2022, pp. 166–171.

[10] L. Galati-Giordano, G. Geraci, M. Carrascosa, and B. Bellalta, "What will wi-fi 8 be? a primer on ieee 802.11bn ultra high reliability," *IEEE Communications Magazine*, vol. 62, no. 8, pp. 126–132, 2024.

[11] A. Mody and G. Stuber, "Synchronization for mimo ofdm systems," in *GLOBECOM'01. IEEE Global Telecommunications Conference (Cat. No.01CH37270)*, vol. 1, 2001, pp. 509–513 vol.1.

[12] Y. Levinbook, D. Ezri, and E. Melzer, "Ap cooperation in wi-fi: Joint transmission with a novel precoding scheme, resilient to phase offsets between transmitters," *Signal Processing*, vol. 220, p. 109432, 2024.

[13] S. Verma, T. K. Rodrigues, Y. Kawamoto, M. M. Fouda, and N. Kato, "A survey on multi-ap coordination approaches over emerging wlans: Future directions and open challenges," *IEEE Communications Surveys & Tutorials*, vol. 26, no. 2, pp. 858–889, 2024.

[14] X. Jiao, W. Liu, M. Mehari, M. Aslam, and I. Moerman, "openwifi: a free and open-source ieee802. 11 sdr implementation on soc," in *2020 IEEE 91st Vehicular Technology Conference (VTC2020-Spring)*. IEEE, 2020, pp. 1–2.

[15] A. Asterjadhi, "Tgbn motions list - part 1 rev. 20," IEEE 802.11 TGbn, Nov 2024. [Online]. Available: https://mentor.ieee.org/802.11/dcn/24/11-24-0171-20-00bn-tgbn-motions-list-part-1.pptx

[16] N. N. Krishnan, E. Torkildson, E. Rantala, I. Seskar, N. Mandayam, and K. Doppler, "D-mimoo – distributed mimo for office wi-fi networks," in *2018 IEEE International Symposium on Dynamic Spectrum Access Networks (DySPAN)*, 2018, pp. 1–10.

[17] D. Nunez, F. Wilhelmi, S. Avallone, M. Smith, and B. Bellalta, "Txop sharing with coordinated spatial reuse in multi-ap cooperative ieee 802.11be wlans," in *2022 IEEE 19th Annual Consumer Communications & Networking Conference (CCNC)*. IEEE Press, 2022, p. 864–870.

[18] P. Imputato, S. Avallone, M. Smith, D. Nunez, and B. Bellalta, "Beyond wi-fi 7: Spatial reuse through multi-ap coordination," *Computer Networks*, vol. 239, p. 110160, 2024.

[19] E. Hamed, H. Rahul, M. A. Abdelghany, and D. Katabi, "Real-time distributed mimo systems," in *Proceedings of the 2016 ACM SIGCOMM Conference*, ser. SIGCOMM '16. New York, NY, USA: Association for Computing Machinery, 2016, p. 412–425.

[20] R. A. Shafik, M. S. Rahman, and A. R. Islam, "On the extended relationships among evm, ber and snr as performance metrics," in *2006 International Conference on Electrical and Computer Engineering*, 2006, pp. 408–411.

[21] "Ad9361 reference manual ug-570," Analog Devices, 2017.

[22] A. Garcia Armada, "Understanding the effects of phase noise in orthogonal frequency division multiplexing (ofdm)," *IEEE Transactions on Broadcasting*, vol. 47, no. 2, pp. 153–159, 2001.

[23] W. Kester, "Converting oscillator phase noise to time jitter," Analog Devices, 2009. [Online]. Available: https://www.analog.com/media/en/training-seminars/tutorials/MT-008.pdf